

Supplementary Note 1: RBD Structural Alignment and Comparison

Using PyMOL's alignment tool (with 50 cycles and a cutoff of 2.0 Å)(30), we superimposed the RBD structures as shown in Figure 6 and show RMSD metrics in Table 6.



Fig. 6. Cartoon representation of the four RBD structures aligned. B.1.1.529 (PDB: 719) in teal, BJ.1 in orange, BM.1.1.1 in purple, and XBB.1.5 in magenta with mutated residues from Table 1 highlighted in yellow.

Variant	B.1.1.529	BJ.1	BM.1.1.1	XBB.1.5
B.1.1.529	0	0.780	0.708	0.653
BJ.1	0.780	0	0.306	0.266
BM.1.1.1	0.708	0.306	0	0.146
XBB.1.5	0.653	0.266	0.146	0

Table 6. Alignment RMSD distance (in Ångstroms) between each variant's RBD structure.

Note that none of the mutations are predicted to disrupt the overall RBD tertiary structure in the AlphaFold2-generated structures. There are minor secondary structure changes as to where alpha helices or the anti-parallel beta sheet may begin or end, but overall the structures are very similar.

Looking at the main loop structure at the top of the S1 region, shown in Figure 7, the residue side chains are in similar positions, differing only by slight angular changes with the exception of the F486P mutation as previously mentioned. This proline mutation does not change the overall loop's conformation, but provides rigidity at this location.

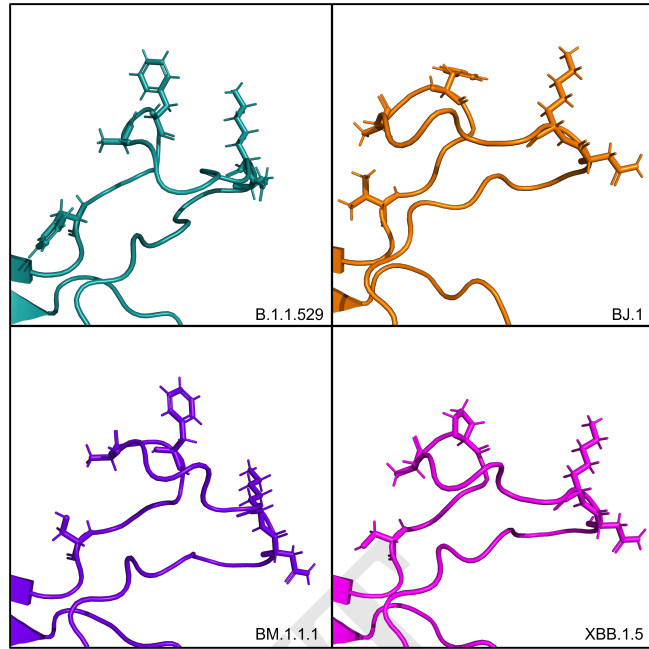


Fig. 7. Side chains of the main loop at the S1 binding site for each of four RBD structures. Residues that are mutated from the wild type reference are shown as sticks.

Supplementary Note 2: RBD Active Residue Predictions

Using CPoRT, an interface predictor that provides a prediction of active and passive residues on a given protein (17), we evaluated the four RBD structures. See Table 7 below.

Variant	Active Residues	Passive Residues
B.1.1.529	357, 359, 360, 361, 390, 391, 394, 417, 452, 453, 455, 456, 457, 470, 471, 476, 478, 479, 481, 482, 483, 484, 485, 486, 487, 489, 490, 492, 493	338, 351, 352, 355, 356, 362, 382, 383, 386, 388, 389, 396, 403, 409, 415, 416, 420, 421, 449, 450, 458, 459, 460, 461, 462, 465, 467, 468, 469, 472, 473, 474, 475, 477, 480, 494, 515, 516, 517, 518, 520, 521, 522, 523, 525, 526, 527, 528
BJ.1	449, 450, 452, 455, 456, 457, 458, 459, 460, 461, 468, 469, 470, 471, 473, 474, 475, 476, 477, 478, 483, 484, 485, 486, 487, 489, 490, 493, 494	345, 346, 347, 351, 352, 403, 417, 419, 420, 421, 422, 444, 447, 448, 453, 462, 463, 465, 466, 467, 472, 479, 480, 481, 482, 495, 496, 497
BM.1.1.1	338, 339, 357, 359, 360, 361, 362, 363, 364, 367, 388, 391, 392, 393, 394, 452, 455, 456, 472, 475, 483, 484, 485, 486, 487, 489, 490, 493, 494	340, 343, 344, 349, 351, 352, 355, 356, 366, 369, 370, 371, 372, 374, 382, 383, 384, 385, 386, 389, 390, 396, 403, 417, 421, 430, 448, 450, 457, 458, 459, 469, 470, 471, 473, 474, 476, 477, 478, 479, 480, 481, 482, 492, 495, 496, 497, 515, 516, 517, 518, 519, 523, 524, 525, 526, 527, 528
XBB.1.5	351, 357, 358, 359, 360, 361, 390, 391, 393, 417, 421, 455, 456, 457, 483, 484, 485, 486, 487, 489, 493, 516, 518, 519, 520, 521, 522, 523, 525	338, 348, 352, 355, 356, 362, 364, 382, 383, 386, 388, 389, 396, 403, 409, 415, 416, 419, 420, 422, 430, 450, 452, 458, 459, 460, 461, 462, 465, 466, 467, 468, 469, 470, 471, 472, 473, 474, 475, 480, 490, 492, 514, 515, 517, 527, 528

Table 7. CPoRT-predicted active and passive residues of the four RBD structures.

Also, if we look at the residues that were predicted to be active visually, we can see that the majority of these residues concentrate around the S1 area of the RBD. Specifically, the loop structure on the top of the RBD that has been discussed heavily in this study and previous works is consistently pre-

dicted to contain multiple active residues across all four variant structures. See Figure 8.

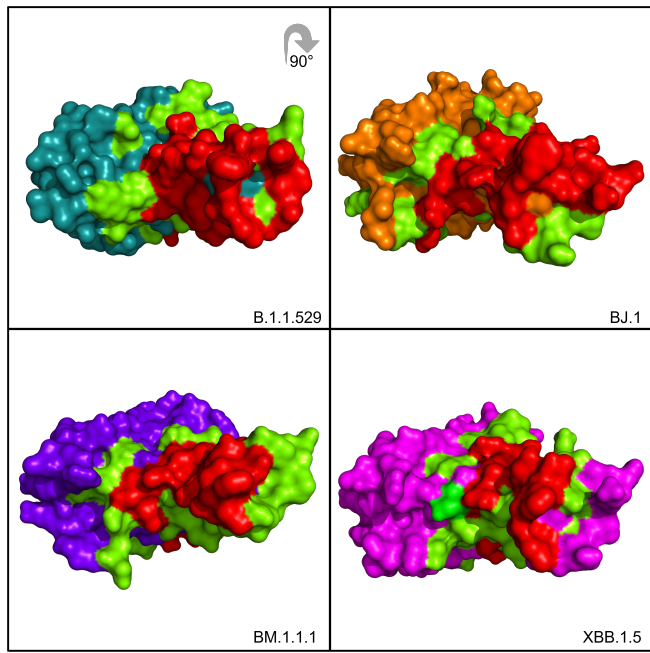


Fig. 8. CPoRT predicted active and passive residues (in red and green, respectively) of the four RBD structures. Shown as the “top” of the RBD, 90° forward.

There is considerable agreement between the CPoRT predictions and the HADDOCK results listed in the main article. Nearly all of the interfacing residues detected in the complexes shown in Figures 3, 4, and 5 are predicted to be active residues from CPoRT. Furthermore, many of these predicted active residues are also mentioned in Jones et al. (14), Westendorf et al. (15) and Dong et al. (16), thus further supporting that these residues on the top of the S1 region stand as the likely epitope between the RBD and various neutralizing antibodies evaluated in this study.

Supplementary Note 3: PRODIGY Results

In Figure 1, we show the top performing antibody-RBD complexes’ HADDOCK and PRODIGY scores. That is, the metrics for the top performing complex from the top performing HADDOCK cluster. In Figure 9 below, we show the individual PRODIGY scores of the top four complexes from the top performing HADDOCK cluster for each antibody-RBD experiment. There is agreement that no statistically significant drop in overall antibody binding affinity in terms of ΔG as predicted by PRODIGY.

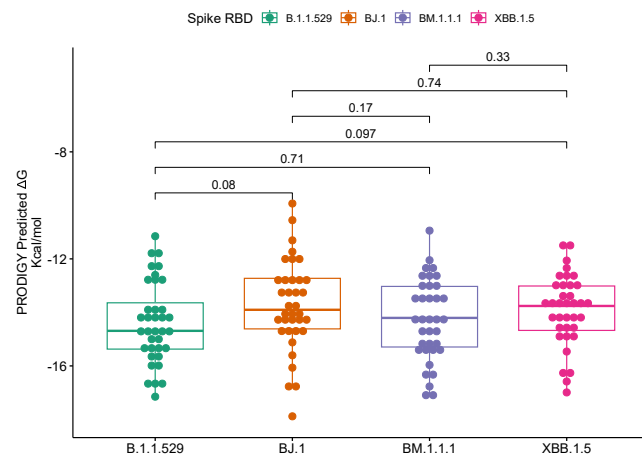


Fig. 9. PRODIGY binding affinity metrics for the top four clusters in each antibody-RBD complex that resulted from the HADDOCK docking process.